Int J Appl Earth Obs Geoinformation 93 (2020) 102196

Contents lists available at ScienceDirect

Int J Appl Earth Obs Geoinformation

journal homepage: www.elsevier.com/locate/jag

Dating flowering cycles of Amazonian bamboo-dominated forests by supervised Landsat time series segmentation

Jasper Van doninck[a], Jan Westerholm[b], Kalle Ruokolainen[c], Hanna Tuomisto[c], Risto Kalliola[a]

[a] Department of Geography and Geology, University of Turku, 20014 Turku, Finland
[b] Åbo Akademi University, Faculty of Science and Engineering, Agora, Vattenborgsvägen 3-5, 20500 Åbo, Finland
[c] Department of Biology, University of Turku, 20014 Turku, Finland

ARTICLE INFO

Keywords:
Amazonia
Bamboo
Change detection
Landsat
Phenology
Time series analysis

ABSTRACT

Bamboo-dominated forests are unusual and interesting because their structure and biomass fluctuate in decades-long cycles corresponding to the flowering and mortality rhythm of the bamboo. In southwestern Amazonia, these forests have been estimated to occupy an area of approximately 160 000 km^2, and a single reproductively synchronized patch can cover up to thousands of square kilometers. Accurate mapping of these forests is challenging, however: the forests are spatially heterogeneous, with bamboo densities varying widely among adjacent sites; much of the area is inaccessible, so field verification of bamboo presence is difficult to obtain and georeferenced records of past flowering events virtually non-existent; and detectability of the bamboo by remote sensing varies considerably during its life cycle. In this study, we develop a supervised time series segmentation approach that allows us to identify both the presence of bamboo forests and the years in which the bamboo flowering and subsequent mortality have occurred. We then apply the method to the entire Landsat TM/ETM+ archive from 1984 to the end of 2018 and validate the classification by visual interpretation of very high resolution imagery. Collecting accurate ground reference data of bamboo presence and bamboo mortality timing is notably difficult in these forests, and we therefore developed a methodology that takes advantage of imperfect reference data obtained from the Landsat time series itself. Our results show that bamboo forests can be differentiated from non-bamboo forests using any of the infrared bands, but band 5 produces the highest classification accuracy. Interestingly, there appears to be a temporal difference in the spectral responses of the three infrared bands to bamboo flowering and mortality: near infrared (band 4) reflectance reacts to the event earlier than shortwave infrared (bands 5 and 7) reflectance. The long Landsat TM/ETM+ archive allows our methodology to detect some areas with two mortality events, with a theoretical maximum interval of 29 years. Analysis of these pixels with repeated mortality confirms that the life cycles of the local bamboo species (*Guadua sarcocarpa* and *G. weberbauerii*) last typically 28 years.

1. Introduction

Although bamboo is often thought typical of Asia, the largest area of bamboo-dominated forests in the world seems to be situated in southwestern Amazonia, where they cover about 160 000 km^2 (de Carvalho et al., 2013). These forests harbor two species of bamboo that are able to reach wide dominance in the forest canopy (*Guadua sarcocarpa* and *G. weberbauerii*, for simplicity collectively referred to as bamboo). Both species share characteristics that make it possible to visually detect bamboo-dominated forests in remotely sensed images. Firstly, since bamboos are grasses, their structure and reflectance are different from those of dicotyledonous trees. Secondly, unlike trees, bamboos have a gregariously semelparous life cycle. This means that bamboo individuals flower and bear fruit just once and then die. The cycle is believed to take about 28 years (de Carvalho et al., 2013), and to be synchronous in large spatially aggregated patches. These patches can cover up to thousands of square kilometres, which makes the alternation between tree-dominated and bamboo-dominated canopy phases clearly visible (Nelson and Bianchini, 2005; de Carvalho et al., 2013; Dalagnol et al., 2018).

The possibility to remotely sense the spatial distribution and temporal dynamics of bamboo forests is important because these forests are hard to access on the ground. This is partly due to sheer distance to roads and navigable rivers, partly because the bamboo itself grows into dense and spiny thickets. A sign of inaccessibility is that several ethnic groups that have retreated to voluntary isolation live in these forests (Kesler and Walker, 2015). Remote sensing studies have already addressed several aspects of bamboo ecology, e.g. quantifying the length of its life cycle and assessing which environmental factors might control the geographical distribution of bamboo-dominated forests (Nelson and

E-mail address: riskal@utu.fi (R. Kalliola).

https://doi.org/10.1016/j.jag.2020.102196
Received 24 April 2020; Received in revised form 17 June 2020; Accepted 10 July 2020
Available online 12 August 2020

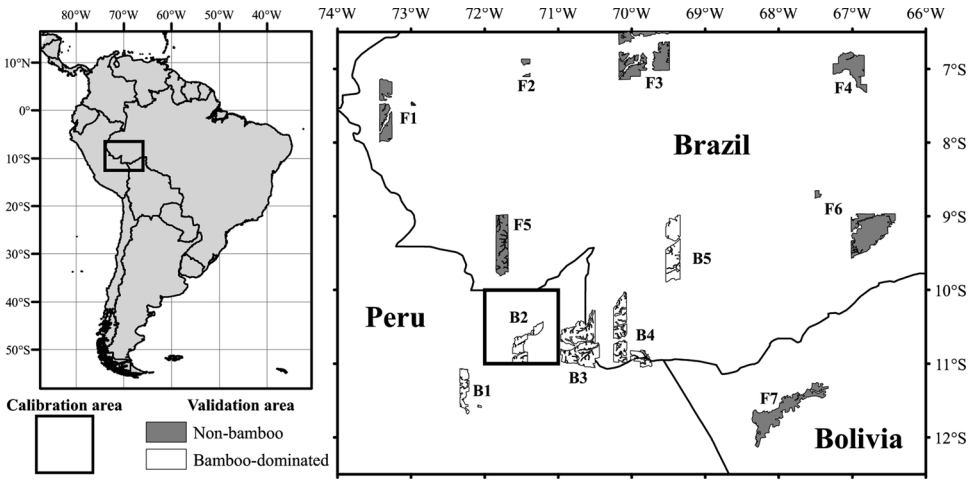

Fig. 1. Location of the study site in South America (left). The black square in the detail of the study site (right) indicates the extent of the calibration area. Grey and white areas indicate validation areas for non-bamboo forests (numbered with prefix F) and bamboo-dominated forests (numbered with prefix B), respectively. The numbering corresponds to Table S1, which lists the acquisition dates of DigitalGlobe images available in GoogleEarth over these validation sites.

Bianchini, 2005; de Carvalho et al., 2013). By overlaying a map of fire occurrences over a map of the timing of the bamboo life cycle, Dalagnol et al. (2018) were even able to address an evolutionary question related to the emergence of a gregariously semelparous life cycle.

The currently available estimates of the geographical distribution of bamboo-dominated forests are based either on automated delimitation using relatively coarse resolution MODIS data (Dalagnol et al., 2018), or on manual mapping of bamboo forest patches in higher-resolution Landsat images (de Carvalho et al., 2013). Both of these come with their specific set of shortcomings. Manual mapping of Landsat imagery is very laborious and subjective, which makes it impractical in applications covering large areas and/or multiple time windows. On the other hand, the minimum size of detectable bamboo patches in MODIS imagery is relatively large due to the coarse pixel size, and since the MODIS instruments were only launched in 1999-2002, the archives do not yet cover a full bamboo life cycle. Nevertheless, a recent study has used MODIS data to derive a prediction of future dynamics in bamboo forests (Dalagnol et al., 2018).

To overcome these problems, a method that combines automatic data processing with high spatial resolution and full coverage of the bamboo life cycle is needed. Landsat TM and Landsat ETM+ images are the most suitable data products for this purpose, because together they span more than three decades at a spatial resolution of 30 m. The adoption of an open data policy in 2008 (Woodcock et al., 2008) resulted in a boom of studies using long Landsat time series (Zhu et al., 2019) and several authors developed and applied Landsat-based methods to detect forest disturbances and dynamics from the tropics to the arctic treeline (Kennedy et al., 2010; Townshend et al., 2012; Banskota et al., 2014; DeVries et al., 2015; Hermosilla et al., 2015; Müller et al., 2016; Bolton et al., 2018).

Although deforestation can now routinely be identified using Landsat time series, identifying low-intensity disturbances correctly remains a challenge (Curtis et al., 2018; Song et al., 2018; Cohen et al., 2017, 2018; Bullock et al., 2020). In particular, the combination of subtle disturbance signals and noisy time series data increases the risk that noise is incorrectly identified as change or actual changes go undetected (Cohen et al., 2018). This is especially a problem within tropical forests, where both data availability and data quality are low, compared to some temperate regions. The reasons for this are varied, such as historic data collection and archiving strategies (Wulder et al., 2016), narrower overlap among adjacent paths close to the equator than close to the poles, persistent cloud cover, variable atmospheric aerosol properties, and sun-sensor geometry effects (Galvão et al., 2011; Nagol et al., 2015; Toivonen et al., 2006). These issues predict low disturbance detecting accuracy for phenomena with a relatively subtle temporal signal of transition, such as that between bamboo-dominated and bamboo-free canopies.

Attempts have been made to increase the accuracy of low-intensity disturbance detection in Landsat time series by incorporating calibration data (Cohen et al., 2018; Schroeder et al., 2017), sometimes combined with a stacking of results of time series segmentations that use different algorithms or different bands (or band combinations) or both (DeVries et al., 2016; Healey et al., 2018; Bullock et al., 2020). The calibration datasets contain information on the exact date and type of disturbance, and they have been obtained by visual assessment of large numbers of pixel time series, e.g. using the TimeSync software (Cohen et al., 2010, 2018; Healey et al., 2018; Schroeder et al., 2017; Pengra et al., 2019) or through community-based sampling efforts (DeVries et al., 2016). A problem with these approaches is that they require a heavy time investment. Additionally, the exact identification of disturbance (mortality) events in bamboo populations from pixel time series may be difficult since preliminary analyses indicate that the spectral response to bamboo mortality in different bands may have different timing.

In this study, we have a number of complementary aims. Firstly, we develop a supervised Landsat time series analysis based on imperfect calibration data to identify, at 30 m resolution, the presence of bamboo-dominated forests and the year in which bamboo dieback has occurred. Secondly, we use these data to assess the temporal duration of the dieback events and the length of the bamboo life cycle. The analysis is based on yearly Landsat 4/5 TM and Landsat 7 ETM+ composite images over the study area between 1984 and 2018, theoretically allowing for the detection of more than a full growing cycle for each bamboo population. Finally, we use Landsat's different infrared spectral bands to evaluate their ability to correctly identify bamboo-dominated forests from their respective temporal patterns, and to assess the spectrotemporal response of bamboo die-back.

2. Study site and data

2.1. Study site

The study area is located in southwestern Amazonia around the triborder area between Brazil, Peru and Bolivia (Fig. 1). The area has a tropical, relatively seasonal climate. The mean annual temperature ranges between 24 and 26°C, and the mean annual rainfall mostly between 1400 mm and 2200 mm, with the driest month receiving 15-40 mm of rain (Karger et al., 2017). Geologically, the area is situated around the Fitzcarrald Arch, and covers the headwater regions of the rivers Ucayali, Juruá, Purus and Madeira.

2.2. Yearly Landsat TM/ETM+ composite images

We used all Landsat 4/5 TM and Landsat 7 ETM+ images that were acquired over the study area from 1984 to 2018 and had a reported

cloud cover percentage below 80 %. We downloaded the images through the USGS/EROS Inventory Service. Temporal Landsat data coverage varied greatly both among and within years. Data availability was highest during the period 1999–2012 when both Landsat 5 and Landsat 7 were operative and especially during the relatively dry season between May and October.

The downloaded images were combined into yearly composites following a methodology similar to the one described in Van doninck and Tuomisto (2018). Individual scenes were first processed to surface reflectance using LEDAPS (Masek et al., 2006) and corrected for the combined effect of topographic and sun-sensor geometry (Flood et al., 2013; Van doninck and Tuomisto, 2017a) using the SRTM digital elevation model. Scenes were then combined into yearly pixel-based composite images using the multidimensional median criterion (Flood, 2013; Van doninck and Tuomisto, 2017b), except when only two observations were available in which case the maximum NDVI criterion was used. We also recorded, for each pixel in each yearly composite image, how many unmasked (cloud- and shadow-free) observations were available to select from. Finally, in order to reduce noise that may result from imperfect georegistration, we applied a band-wise spatial filter over each one of the yearly composite images separately. In the filtered image, each pixel was assigned the median value of the 3x3-pixels window centred on the original pixel.

Combining the images into yearly composites helped to reduce the problem of missing data and make the time series more uniform, and can be expected to improve the signal-to-noise ratio (Van doninck and Tuomisto, 2017b). Intra-year phenology is relatively weak in Amazonia, and few images in the time series were obtained during the period November–April. Therefore, we chose to forego an analysis of intra-year vegetation phenology. The multidimensional median composition criterion selects the observation that is most representative for the corresponding yearly time window, and this can be assumed to generally have been acquired during the relatively cloud-free season from May to October. Even though we allowed up to 80 % cloud cover in the selected images, several yearly composites in the time series showed areas of missing data, meaning that none of the images acquired in that year had cloud-free observations for those pixels. Missing data was especially a problem for the years prior to the launch of Landsat 7 and its ETM+ sensor in 1999 (Fig. 2).

2.3. Calibration and validation data

Reliable calibration and validation of Landsat time series analysis for detecting bamboo mortality events require a sizeable amount of reference data. We carried out field work on two occasions, but the area is extensive and difficult to access, so this only covered a few sites. In general, in situ data on the presence or absence of bamboo populations in Amazonia is scarce, and even less is known about their dates of mortality or other phenological phases. We therefore collected the extensive calibration and validation data needed for this study from remotely sensed imagery.

We collected calibration data through visual interpretation of the Landsat time series itself. For an area of one by one degree (Fig. 1), we digitized polygons of bamboo-dominated forests and non-bamboo forests, and estimated the dates of mortality for the bamboo populations (Fig. 3). Digitization was based on false-colour composite images assigning three consecutive years of a single spectral band to the three colour channels. If the three selected years covered a mortality event for a population, that patch lighted up in colour against the greyscale colours of stable bamboo or non-bamboo forests, and a polygon around that population was drawn and the year of mortality was assigned to the polygon. Some uncertainty exists on the estimated mortality dates because of the often subtle reflectance changes associated with bamboo mortality, and slight differences in interpretation result when assessing the different infrared bands. Due to lack of in situ reference data, it was impossible to assess the quality of the digitization. Because of the used

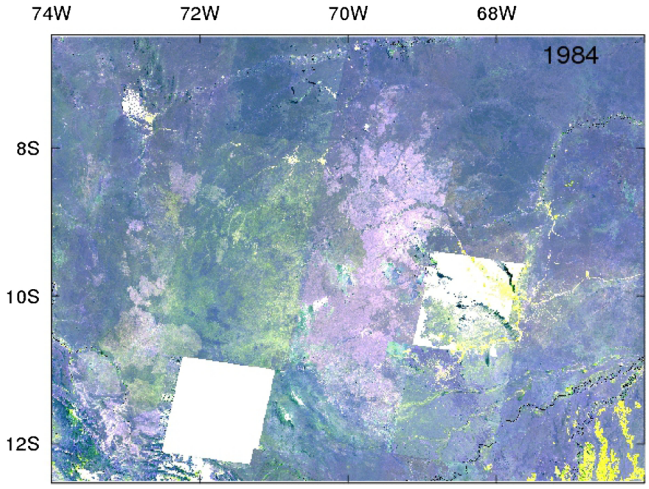

Fig. 2. Yearly Landsat false-colour composite based on all TM and ETM+ images acquired in 1984 with less than 80 % cloud cover (print); time series of yearly Landsat false-colour composites based on all TM and ETM+ images acquired from 1984 to 2018 with less than 80 % cloud cover (online). Red, green and blue colour channels correspond to short-wave infrared 1 (SWIR1), SWIR2 and near infrared (NIR), respectively.

digitization technique, however, we are confident that the assigned dates were within two years of the actual disturbance. Furthermore, the digitized polygons were spatially coarser than Lansdat's 30 m resolution since it was practically infeasible to digitize at the scale of the individual pixel over a 1˚ by 1˚ area. A non-negligible number of pixels may therefore have been assigned to the wrong polygon. While we acknowledge that the quality of reference data obtained in this way may be lower than data collected by interpretation of individual pixel time series through, e.g. TimeSync (Cohen et al., 2010), our methodology allows for the collection of far more reference data points using limited resources. We delineated validation areas of bamboo-dominated forests and non-bamboo forests by visual interpretation of DigitalGlobe images, available through Google Earth (Fig. 1, Table S1). We aimed at including only *terra firme* forests in these validation areas by excluding apparent flood plains of even relatively small rivers. Bamboo-dominated forest stands are separable from other forest types by their distinct combination of texture and colour in these very high spatial resolution images (Fig. S1). Bamboo can be hidden in these images over a significant proportion of an area where it is present because tree canopies can overshadow even full-grown bamboo. Accordingly, we delimited the bamboo validation areas such that we allowed for the presence of even several hectares of continuous cover of forest trees as long as bamboo was regularly visible. The total area of polygons identified as bamboo-dominated and non-bamboo forests are 7 599 km^2 and 12 141 km^2, respectively.

3. Methodology

We developed a two-stepped time series segmentation to detect areas of bamboo-dominated forests and the start date of mortality events. An overview of the method is given in Fig. 3 . In the first step, we applied an unsupervised segmentation on the basis of knowledge on bamboo biology. Results of this first segmentation were then compared to the visual interpretation over the calibration area (Fig. 1). Because of the high noise level in the Landsat time series and the subtle disturbance signal, we expected a poor classification accuracy for this unsupervised segmentation. Therefore, the output parameters from the first segmentation and the visual interpretation together were used to calibrate a support vector machine (SVM) classifier. This classifier was then integrated into the second, supervised segmentation. Finally, pixel-based results

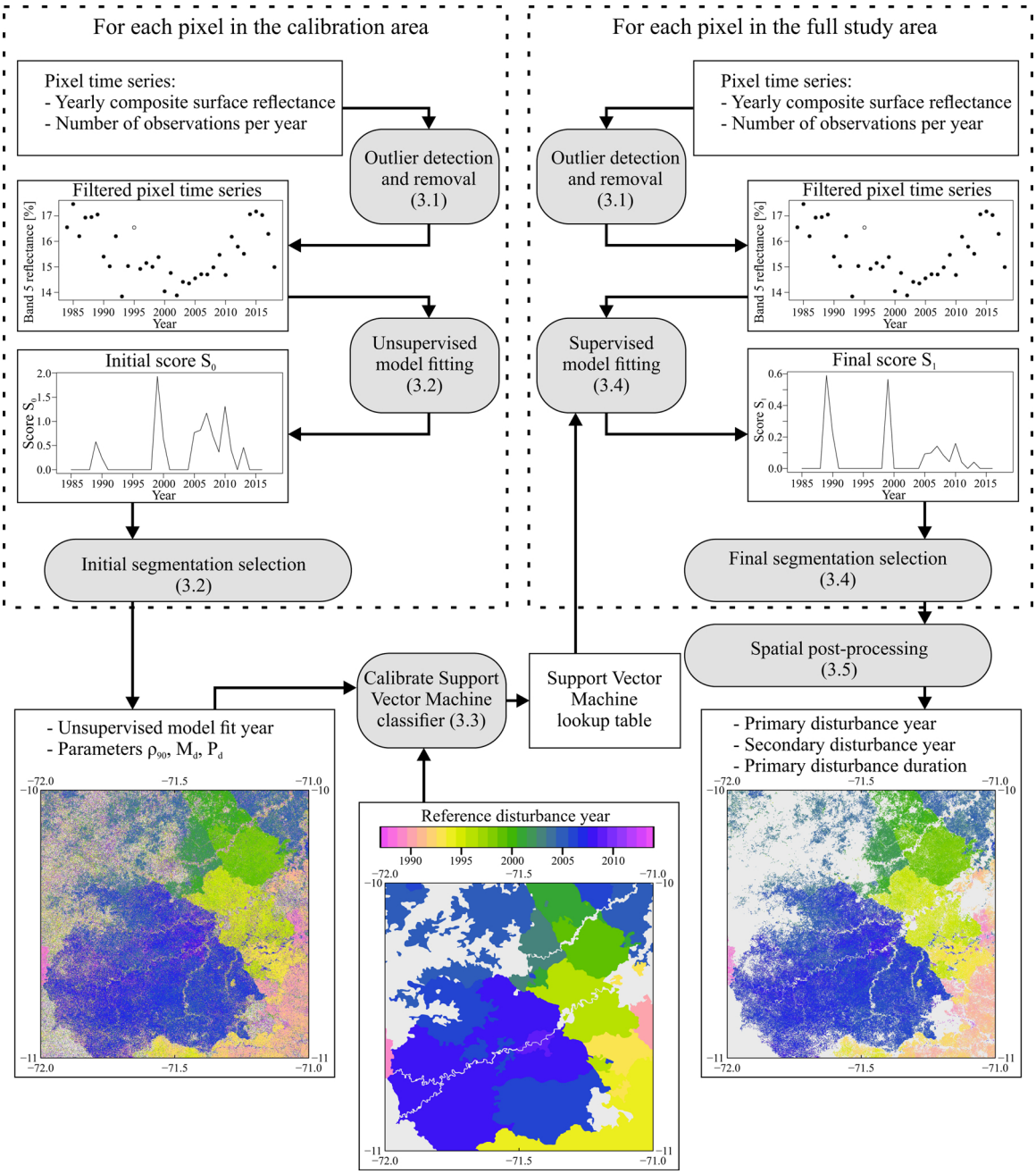

Fig. 3. Flowchart of supervised time series segmentation for the pixels of yearly Landsat image composites using a single band (here SWIR1). Numbers in parentheses indicate in which section of the text the corresponding processing step is explained.

were combined in a spatial post-processing, and a disturbance signal-to-noise ratio was calculated.

In order to assess the spectrotemporal response of bamboo die-back, the entire analysis chain was executed separately for each of the three infrared Landsat TM/ETM+ bands: NIR (near infrared, band 4), SWIR1 (shortwave infrared, band 5), and SWIR2 (band 7). Strong atmospheric contamination over Amazonia results in noisy data in the visible Landsat bands 1, 2 and 3 (Van doninck and Tuomisto, 2017b), and we therefore excluded these bands and spectral indices using them (e.g., Normalized Difference Vegetation Index, Tasseled Cap transformation). Previous studies have suggested, and our preliminary analyses confirmed, that bamboo mortality causes a decrease in surface reflectance across the near and shortwave infrared spectrum (de Carvalho et al., 2013; Dalagnol et al., 2018). Band indices or ratios combining infrared bands (e.g., Normalized Burn Ratio) are therefore less suitable for discrimination between forests with and without mature bamboo, and we did not consider them for analysis.

3.1. Outlier detection and removal

Outliers were identified for each pixel time series and each band separately by two consecutive detection methods. First, we used a global method to detect the most obvious outliers caused by residual clouds or cloud shadow. This was done by identifying the observation in the time series which had the largest absolute departure from the mean value over the time series. If this difference was larger than three times the standard deviation of the entire time series, the observation was flagged as an outlier and removed from the time series. This process was repeated until no more global outliers were identified. In the second step, a local method identified more subtle outliers resulting,

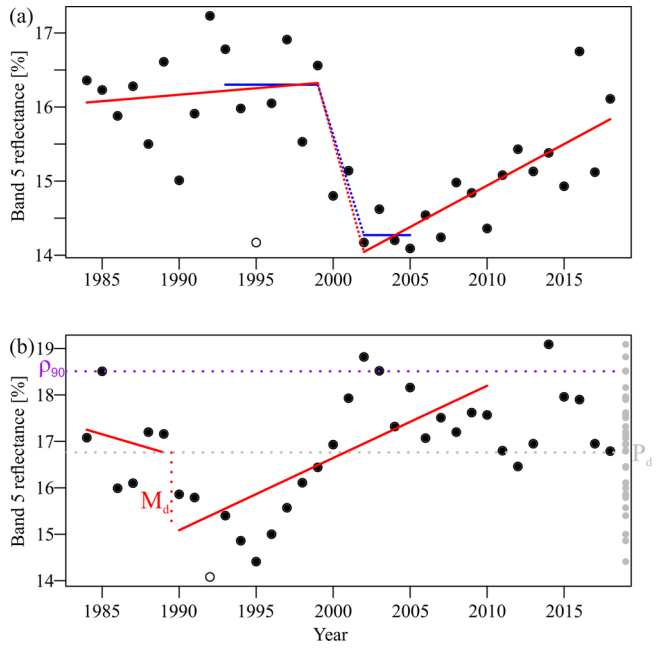

Fig. 4. Example time series for two pixels. Full circles indicate observations used in the time series segmentation, open circles indicate observations flagged as outliers. (a) Time series with spectral disturbance starting in 1999 and with a duration of three years. Full red and blue lines indicate linear and constant model fit, respectively, before and after the start of the disturbance, dashed red and blue lines indicate linear interpolation for the duration of the disturbance for the respective models. (b) Time series with spectral disturbance starting in 1989 and duration of one year, with indication of the 90th percentile of the time series (ρ_{90}), magnitude of the disturbance (M_d), and percentile of the start of the disturbance within the values of the time series (P_d).

e.g., from haze, smoke or other uncorrected atmospheric effects. Each observation in the yearly pixel time series was compared to the preceding and following observations within a temporal window. For each observation i, a score τ_i was calculated as:

$$\tau_i = \frac{|\rho_i - \bar{\rho_w}|}{\sigma(\rho_w)}\omega_i, \quad (1)$$

where ρ_i is the surface reflectance in the processed band for year i, $\bar{\rho_w}$ and $\sigma(\rho_w)$ are the mean and standard deviation of surface reflectance values for the adjacent observations within the temporal window, respectively, and ω_i is a weighting parameter. When using multi-dimensional median compositing the uncertainty on the pixel-based composite is expected to decrease with the number of available observations per pixel within the compositing period (N_i), following roughly an exponential decay function (Van doninck and Tuomisto, 2017b). We therefore defined ω_i as:

$$\omega_i = e^{-\lambda(N_i-1)}, \quad (2)$$

where λ is the exponential decay constant. The observation in the time series with the largest τ_i was selected, and if this value was larger than a critical value τ_c, the observation was flagged as a local outlier and removed from the time series. This process was repeated until no more local outliers are identified. Like many other methods, this noise removal approach requires a number of a priori determined parameters, in this case the critical value τ_c, the exponential decay constant λ, and the size of the temporal window around each observation. After manual assessment for a number of pixels, we set $\tau_c = 2$, $\lambda = 0.25$, and the window size at three years on each side of each observation. If more than 25 % of the yearly observations in the resulting filtered pixel time series were missing, the pixel was not further processed. A "no data" value was then assigned to that pixel in all output products.

3.2. Unsupervised model fitting and initial segmentation selection

Unsupervised model fitting for each infrared band separately was based on two assumptions based on the known bamboo ecology and the spectral response of bamboo die-off and regrowth. Firstly, it was assumed that for a longer period of time between two mortality events, surface reflectance of bamboo-dominated forests can be described by a linear model. This pattern arises when bamboo gradually increases in abundance and starts to dominate the forest canopy and its reflectance, and it was the basis of the model fitting in a previous study (Dalagnol et al., 2018). Secondly, results by Dalagnol et al. (2018) using MODIS data showed that surface reflectance over bamboo-dominated forests could be considered constant for a shorter period of time both before and after a bamboo mortality event. This is because bamboo plants reach full stature already a few years before flowering and mortality, and a few years are required before the young bamboo plants have grown large enough to influence the remotely sensed signal from the forest canopy.

Based on these two assumptions, we defined an initial score S_0 as the product of a short-period constant fit improvement and a long-term linear fit improvement after segmentation:

$$S_0 = \frac{\mathrm{SSE}^o_{\mathrm{const}} - \mathrm{SSE}^s_{\mathrm{const}}}{\mathrm{SSE}^s_{\mathrm{const}}} \frac{\mathrm{SSE}^o_{\mathrm{lin}} - \mathrm{SSE}^s_{\mathrm{lin}}}{\mathrm{SSE}^s_{\mathrm{lin}}}, \quad (3)$$

where *SSE* stands for the sum of squared errors, the subscripts *const* and *lin* indicate the constant and linear regression model fit, respectively, and the superscripts *o* and *s* indicate the original and segmented model fit, respectively. The score S_0 was calculated for each observation in the pixel time series, except the first and the two last ones in order to assure that segments consist of at least two observations. We defined the two short constant periods, before and after mortality, to last for up to six observations each, and the two linear periods to last for up to twenty observations each. The original constant model was thus fitted to the six observations leading up to the target year, or to all observations from the start of the time series if this was the smaller number, and the six observations following the target year, or all observations to the end of the time series if this was the smaller number. Similarly, the original linear model was fitted to the twenty observations leading up to and twenty observations following the target year, if there were more than twenty observations before reaching the beginning or end of the time series. The segmented models were then fitted separately to observations leading to and following the target year.

The spectral response to a vegetation disturbance event is not necessarily instantaneous and can span a period of more than one year. We therefore allowed the discontinuity following the target year to be of a duration of either one, two or three observations. In the latter two cases, the constant or linear model for the segment following the considered year were only fitted for the second or third observation, respectively, up to the last observation of that segment. The one or two intermediate observations were then fitted through linear interpolation (Fig. 4 (a)). For each year, the duration of the discontinuity was then defined by selecting the case resulting in the highest score S_0. Regardless of the duration of the discontinuity, we allowed no more than a single year to have a missing observation during this period. Therefore, the actual duration of the spectral discontinuity could be registered as up to four years.

For each considered observation (second until third to last), the Chow statistic (Chow, 1960) of the segmentation for both the constant and linear model was calculated. If the p-value of either of these was larger than 0.05, the initial score S_0 corresponding to that observation was set to zero. As the initial segmentation for the pixel time series, we then selected the year corresponding to the largest value of S_0. If S_0 was zero for all observations, the pixel was labelled as non-bamboo forest. For those pixel time series for which a statistically significant segmentation was identified, we registered the year corresponding to the

maximum S_0 as the unsupervised model fit year (Fig. 3).

3.3. Calibration of the Support Vector Machine classifier

We randomly selected 100 000 pixel time series from the calibration area (Fig. 1) and compared the results of the initial segmentation with the visual interpretation of the calibration area. After removing those pixels for which no statistically significant initial segmentation was obtained, the remainder could be assigned to three groups: pixels that were located in the area defined as non-bamboo forests in the visual interpretation; pixels that fell within the area defined as bamboo-dominated forests in the visual interpretation and for which the year with the maximum S_0 score was within an error margin of two years of the year visually identified as the mortality; and pixels that fell within the area defined as bamboo-dominated forests in the visual interpretation but with the year of maximum S_0 outside the two year error margin. We defined the first two of these groups as false positive samples and true positive samples, respectively and subsampled the larger of the two to obtain a balanced set. These were then used to calibrate a Support Vector Machine (SVM) classifier. Predictive variables were a set of three parameters extracted from the selected initial time series segmentation (Fig. 4 (b)): the 90th percentile of the observations in the time series (ρ_{90}), the magnitude of the disturbance modelled by the linear fit (M_d), and the percentile of the start of the disturbance modelled by the linear fit within the values of the time series (P_d). We selected these parameters because we assumed bamboo mortality causes, for each spectral band, a disturbance of a typical magnitude and sign, surface reflectance before disturbance is typically at an extreme end of the time series, and maximum reflectance over time of bamboo-dominated forests is typically different from that of non-bamboo forests.

We used a SVM with a radial based function (RBF) kernel, which requires setting two parameters: gamma and cost. These were set at 0.5 and 0.25, respectively, since parameter tuning showed that classification accuracy was rather insensitive to a wide range of RBF gamma and cost parameters. The calibrated SVM was then used to create a lookup table for the range of the three predictor variables in the calibration set and with intervals of 0.0005 (reflectance units) for ρ_{90} and M_d, and 0.05 for P_d.

3.4. Supervised model fitting and final segmentation selection

In the supervised model fitting, we combined the information gained from the calibrated SVM with the unsupervised model fit. After global and local outlier detection and removal, the initial score was again calculated for each observation in the pixel time series following section 3.2 and Eq. (3), starting from the second observation up to the third to last, as well as the corresponding parameters ρ_{90}, M_d and P_d. We then used the calibrated SVM lookup table to obtain the probability P (ρ_{90}, M_d, P_d) that the model fit at each observation in the pixel time series reflects a bamboo mortality event. This leads to a final score S_1 for each observation, defined as:

$$S_1 = P(\rho_{90}, M_d, P_d) S_0. \quad (4)$$

This formulation ensures that the highest value of S_1 corresponds to an observation that combines a strong improvement in constant and linear model fit after segmentation, with a set of disturbance parameters that reflect bamboo mortality. In analogy to section 3.2, values of S_1 were set to zero at observations for which the p-value of the Chow statistic for the constant or linear model fit was higher than 0.05. Additionally, S_1 was set to zero at observations for which the corresponding $P(\rho_{90}, M_d, P_d)$ was below 0.5. If, after these operations, all values of the final score for a pixel were zero for the time period 1987–2014, the pixel was labelled non-bamboo forest. Otherwise, the pixel was classified as bamboo-dominated forest, and the year of the observation corresponding to the largest value of S_1 was identified as the start year of the primary disturbance event. The duration of the disturbance (Fig. 4 (a)) for the observation with maximum S_1 was also written to file. A pixel was labelled as having a secondary disturbance event if one or more non-zero values remained for any of the observations within the time period 1985–2016 and at least 20 years removed from the observation of primary disturbance. The year with the highest value of S_1 among these was then identified as the secondary disturbance year.The period for observation of the primary disturbance year was restricted to 1987–2014 because this corresponds to the 28 years earlier reported as the duration of the *Guadua spp* flowering cycle. Additionally, this reduced the chance that either of the segments after segmentation covered only two observations. In case both the primary and the secondary disturbance year were within the period 1987–2014 and the primary disturbance year was after the secondary, they were switched.

3.5. Spatial post-processing and calculation of disturbance signal-to-noise ratio

Following our methodology, it is possible that the first year after the observation identified as the start of a disturbance event corresponds to a missing observation. This introduces an ambiguity in defining the year of bamboo mortality. We used a spatial analysis to mitigate this ambiguity, where each pixel where this situation occurred was compared to its four nearest neighbours. If at least one of these four pixels was assigned the same primary disturbance year, but did not have a missing observation the next year, this initial year was confirmed. If not, we checked whether at least one of the adjacent pixels had a primary disturbance date one year later while not having a missing observation the next year. In that case, we added one year to the disturbance year of the considered pixel. After checking this for all ambiguous pixels, this process was repeated until no more pixels were updated.

In a final step, we masked non-forested pixels using the global forest change map of Hansen et al. (2013), and removed clusters of pixels labelled as bamboo-dominated forests if they were smaller than the minimum mapping unit. The minimum mapping unit was set to 28 connected pixels (four neighbour connectivity), which corresponds to approximately 2.5 ha.

Calculation of the disturbance signal-to-noise ratio (DSNR) was inspired by the metric proposed by Cohen et al. (2018), adjusted to the supervised segmentation approach used in our study. As in Cohen et al. (2018), it is obtained by dividing spectral difference across the full length of the disturbance by the root mean square error (RMSE) of the residuals:

$$\mathrm{DSNR} = -\frac{M_d}{\sqrt{\frac{\mathrm{SEE}^S_{\mathrm{lin}}}{n}}}, \quad (5)$$

where we define as signal the magnitude of the disturbance according to the linear model (M_d, Fig. 4 (b)), and the residuals are obtained from the n observations used to fit the linear model.DSNR was calculated for 100 000 randomly selected pixels in the calibration area (Fig. 1, Fig. 3) that were correctly classified as bamboo-dominated forests, and had the modelled date of disturbance within two years of the year of mortality as estimated from visual interpretation of the calibration area. The metric was calculated for the three spectral bands NIR, SWIR1 and SWIR2.

4. Results

4.1. Data availability

Any interpretation of the results of the time series analysis cannot be seen independently from the availability of data on which the analysis is based. Missing data points in the Landsat time series include years for which no (cloud-free) Landsat acquisitions were available, and those observations masked as outliers in the multitemporal analysis. The number of missing observations and the maximum number of consecutive years without observation (Fig. 5) clearly highlight data scarcity for some WRS-2 scenes, as well as permanent cloud cover over the Andean foothills in the southwestern part of the study site.

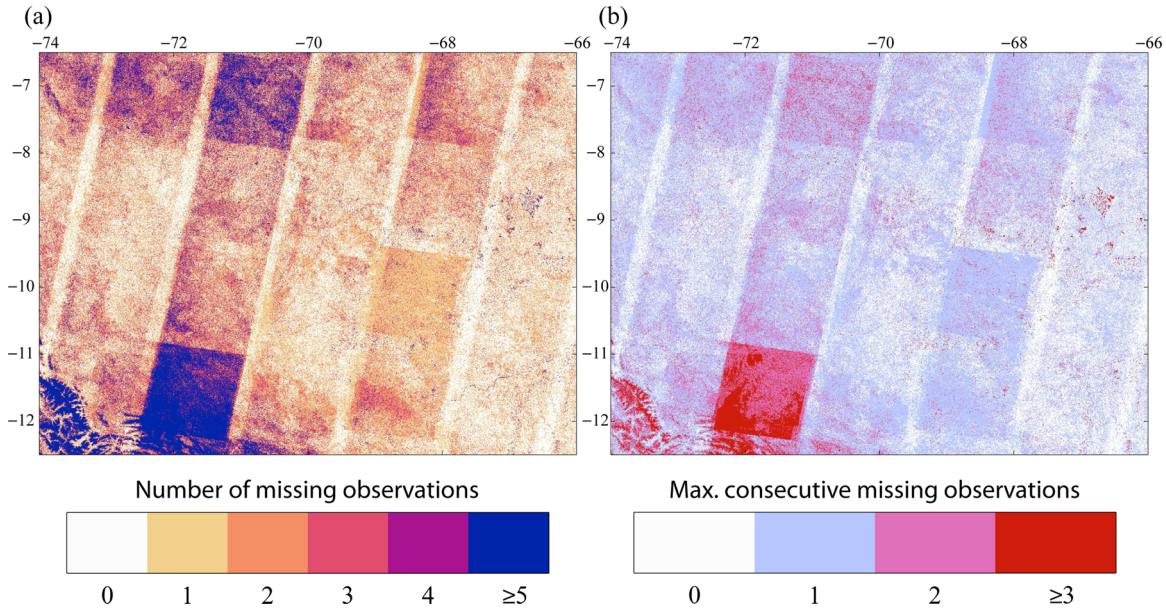

Fig. 5. Number of years with missing or filtered observations in Landsat SWIR1 band per pixel for the period 1984–2018 (a). Maximum number of consecutive years with missing or filtered observations in Landsat band 5 per pixel for the period 1984–2018 (b).

4.2. Classification accuracy and disturbance signal-to-noise ratio

Comparison of the first, unsupervised time series segmentation of the SWIR1 band with the visual interpretation over the calibration area in a confusion matrix (Table 1) shows that of 100 000 randomly selected pixels, only 57 % were correctly classified as either non-bamboo forest or bamboo forests with date of mortality within the 2-year margin. A majority (67 %) of the non-bamboo pixels were labelled as bamboo, and 29 % of the bamboo pixels were labelled as such but had a disturbance date outside of the 2-year margin. The large misclassification of noise as disturbances can also clearly be seen in the detail of the unsupervised model fit in Fig. 3 . After the second, supervised segmentation, the number of non-bamboo pixels for which noise was attributed to change was drastically reduced to only 6 % (Table 1). Also the number of bamboo pixels that were assigned a wrong disturbance date dropped drastically, although most of these were classified as non-bamboo in the second step.

Validation using the high resolution imagery available in Google Earth (Fig. 1, Fig. S1, Table S1) revealed that the Landsat SWIR1 band succeeded much better in discriminating bamboo-dominated forests from non-bamboo forests than the other infrared bands did (Table 2).

Table 1
Confusion matrices of validation of the unsupervised and supervised segmentation using the SWIR1 band and 100 000 pixels over non-bamboo forests (0) and bamboo-dominated forests (1) in the visual interpretation of the calibration area. For those pixels assigned to bamboo-dominated forests in both the calibration dataset and the prediction, we subdivided the pixel count based on the absolute difference between disturbance date assigned by visual interpretation and prediction ($|\Delta Y|$) Pixels indicated with * and ** were used for training of the support vector machine classifier.

	Unsupervised			Supervised		
	Reference					
Prediction	0	1		0	1	
0	7 087		5 447	20 091		24 969
1	14 301*	$\|\Delta Y\| = 0$	14 895**	1 297	$\|\Delta Y\| = 0$	13 337
		$\|\Delta Y\| = 1$	25 532**		$\|\Delta Y\| = 1$	23 744
		$\|\Delta Y\| = 2$	9 602**		$\|\Delta Y\| = 2$	8 741
		$\|\Delta Y\| \geq 3$	23 136		$\|\Delta Y\| \geq 3$	7 821

Especially the omission errors of the NIR and SWIR2 bands were high, above 50 %, compared to only 27.62 % for the SWIR1 band. Commission errors for NIR and SWIR2 (7.8 % and 6.7 %, respectively) were also notably higher than for SWIR1 (4.3 %).

The higher classification accuracy for the SWIR1 band corresponded to a higher median disturbance signal-to-noise ratio over the calibration area (0.75), compared to the NIR (0.61) and SWIR2 (0.55) bands (Fig. 6). While the signals detected using the NIR band (median value of magnitude of -3.82 %) were much larger than those in the SWIR1 and SWIR2 (-1.99 % and -0.81 %, respectively), the near infrared also suffers from a much higher noise level.

Figure 7 shows the extent of the area classified as bamboo-dominated forests and the start year of the disturbance segment for the SWIR1 band. Individually processed pixels cluster into patches of similar mortality date for sometimes large areas. Several examples of ”flowering waves“ can be observed, where adjacent bamboo populations show a mortality in adjacent or proximate years (de Carvalho et al., 2013). The total area identified as bamboo-forest using SWIR1 measures approximately 118 000 km^2.

Table 2
Confusion matrices for classification of bamboo-dominated forests (1) and non-bamboo forests (0), percentage of correctly classified pixels (PCC), and Cohen's kappa coefficient (κ), for the three infrared Landsat bands. The locations of the validation areas for bamboo and non-bamboo forests based on very high resolution DigitalGlobe imagery are shown in Fig. 1 .

	Reference		PCC	κ
Prediction	NIR			
	0	1		
0	12 061 050	4 144 945		
1	338 416	3 988 582		
			78.17	0.5036
	SWIR1			
	0	1		
0	12 136 075	2 246 383		
1	263 391	5 887 144		
			87.78	0.7333
	SWIR2			
	0	1		
0	12 115 266	4 152 103		
1	284 200	3 981 424		
			78.39	0.5082

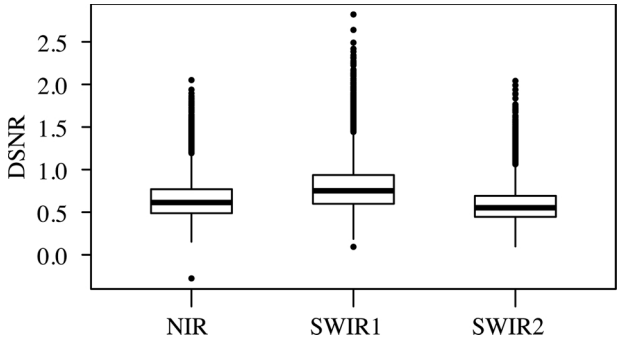

Fig. 6. Boxplots of disturbance signal-to-noise ratio (DSNR) for Landsat NIR (band 4), SWIR1 (band 5) and SWIR2 (band 7). Boxes indicate the interquartile ranges, thick lines the median values.

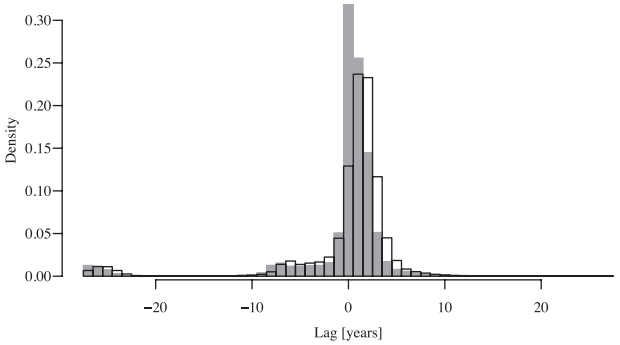

Fig. 8. Histogram of difference between start year of disturbance segments in the three infrared bands. Shaded bars = NIR-SWIR1 difference, outlined bars = NIR-SWIR2 difference.

4.3. Mortality lag and cycle length

Comparison of the disturbance years for those pixels that were identified as bamboo forests in all three infrared bands revealed that the timing of the disturbance rarely coincides for the three bands (Fig. 8). Typically, disturbances in the shortwave infrared bands lagged behind on the disturbance in the near infrared band, with SWIR2 showing an additional lag on SWIR1.

For those pixels for which two disturbance events were identified in all three bands, we also calculated the difference between the start years of the disturbance segments (Fig. 9). This can be interpreted as the length of the phenological cycle of bamboo growth, flowering and mortality. This cycle length was between 27 and 29 years for the vast majority of pixels, with a length of 28 years being dominant for the analysis using the SWIR2 band. Given our methodology and the length of the entire Landsat time series (1984–2018), the theoretical maximum cycle length is 29 years, and the minimum was set to 20 years.

4.4. Duration of the spectral disturbance

The time series analysis method returns the length of the disturbance segment of the model fit resulting in the highest score, for each pixel labelled as bamboo-dominated forest. We report this in Fig. 10 for the SWIR1 band, which has the highest overall classification accuracy. Figure 11 shows the number of pixels with a primary disturbance for each year, subdivided by the length of the disturbance segment. These figures show that the duration of the disturbance is best described by a segment longer than a single year for a majority of the pixels in the study area. The length of the disturbance segment is often spatially clustered (Fig. 10), revealing patterns similar to those of the start year of the segment (Fig. 7). The majority of the pixels have a mortality event occurring in the late 1980's and early 1990's (Fig. 11), many of these being located in the large, central-northern area shown in purple colours in Fig. 7 .

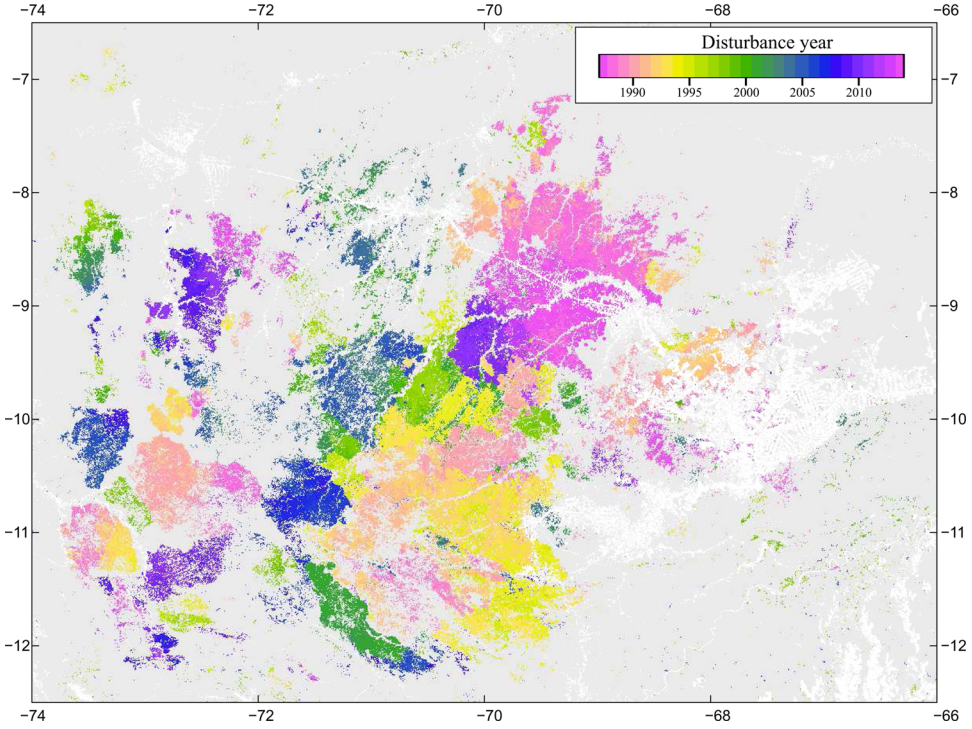

Fig. 7. Start year of the primary disturbance event in bamboo-dominated forests for Landsat SWIR1 band. Grey areas indicate pixels classified as non-bamboo forests. Non-forest pixels (according to Hansen et al. (2013)) are masked out in white. Pixels for which the disturbance segment contained more than one missing observation were classified as non-bamboo forests.

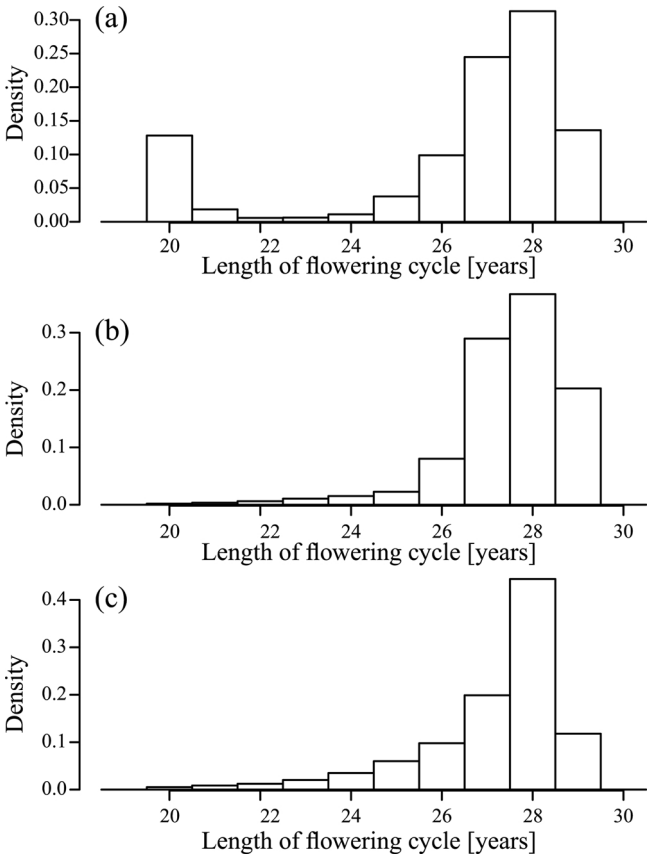

Fig. 9. Length of bamboo phenological cycles, defined as the time between two disturbance events in Landsat NIR (a), SWIR1 (b) and SWIR2 (c) bands. Given the length of the available Landsat time series, the maximum detectable cycle length is 29 years.

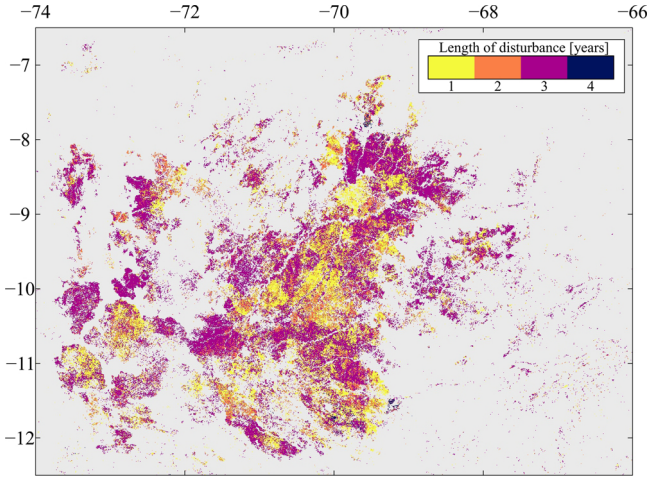

Fig. 10. Length of the disturbance event in bamboo-dominated forests for Landsat SWIR1 band. Grey areas indicate pixels classified as non-bamboo forests, or identified as non-forest pixels (according to Hansen et al. (2013)). Pixels for which the disturbance segment contained more than one missing observation were classified as non-bamboo forests.

The breakdown of the length of the disturbance events varied strongly between spectral bands when considering those pixels identified as bamboo-dominated forests in all three infrared bands. Using the SWIR1 band, only 25 % of the bamboo pixels were best modelled using a disturbance segment of a single year. This number was much higher in the NIR (43 %) and SWIR2 (39 %) bands.

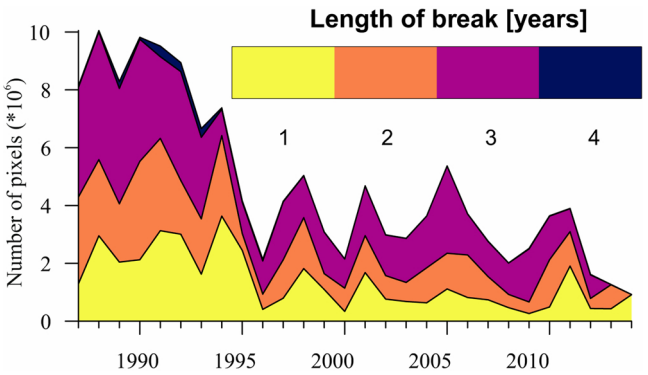

Fig. 11. Number of pixels with primary disturbance event for each start year, subdivided in length of the disturbance event.

5. Discussion

Due to their enormous spatial extent and difficult accessibility, the only realistic way to map bamboo-dominated forest in southwestern Amazonia is through remote sensing. Previous studies with this goal used visual interpretation of Landsat images (de Carvalho et al., 2013) or automated mapping using MODIS time series (Dalagnol et al., 2018). This study is the first attempt to map the Amazonian bamboo forests through a supervised time series segmentation of the entire Landsat archive. Our results show that of the three infrared Landsat TM/ETM+ bands, SWIR1 is the most useful for mapping bamboo populations, resulting in the highest classification accuracy (Table 2) and largest disturbance signal-to-noise ratio (Fig. 6). This contradicts previous studies, which claim that the near-infrared band is more suitable (de Carvalho et al., 2013). Overall, DSNR is low for all three infrared Landsat bands. In a study over American forests it was found that DSNR of forest disturbance events can be increased significantly when the NIR band is combined with either of the SWIR bands into a spectral index (Cohen et al., 2018). This is, however, only the case if a forest disturbance event results in a decreased NIR reflectance (less photosynthetically active vegetation) combined with an increased SWIR reflectance (less water absorption by vegetation), or vice versa. The mortality of bamboo patches, conversely, results in a decrease of surface reflectance throughout the near and shortwave infrared wavelengths.

Even for the SWIR1 band, a relatively large omission error remains (28 %), compared to commission errors. The total area classified as bamboo-dominated forests of 118 000 km^2 (Fig. 1) is therefore possibly underestimated, which explains the difference with previous estimates of the bamboo extent of 160 000 km^2 (de Carvalho et al., 2013). Part of the omission error, and the discrepancy with previous studies, can be attributed to the way the pixel-based time series analysis method is validated using polygons based on very high resolution satellite imagery. These polygons were digitized to encompass large areas of bamboo-dominated forests (Fig. 1). However, these areas are not homogeneous, and may be composed of denser and less dense areas of *Guadua* bamboo within these forests (see Fig. S1). One or a few clustered large trees may prevent the bamboo grasses from dominating the canopy, and hide the temporal bamboo signal. Stated differently: not every pixel in bamboo-dominated forests has a canopy dominated by bamboo. A re-labelling of these small clusters of pixels classified as non-bamboo forests to bamboo-dominated forests may result in a decrease of omission errors. We, however, chose not to do this since it would introduce ambiguity about which disturbance year to assign to these pixels.

Disturbances resulting from bamboo mortality are typically assigned a later date when the analysis is based on the SWIR bands compared to when it is based on the NIR band (Fig. 8). This means that, despite resulting in a higher classification accuracy, SWIR1 may not be the optimal band to identify the exact date of mortality of a bamboo

population. Rather, SWIR reflectance changes seem to indicate a post-mortality signal. This behaviour is also apparent in the results obtained using MODIS by Dalagnol et al. (2018), though they didn't specifically address this. We hypothesise that the delayed response in the SWIR wavelengths is because after mortality, dead bamboo plants remain in the canopy for some time, thus resulting in a high surface reflectance in bands sensitive to leaf water content (de Carvalho et al., 2013). After decomposition of these dead plants, surface reflectance will be influenced by canopy trees and (pioneer) understory vegetation with higher leaf water content. This can also explain why the duration of the modelled disturbance is often longer than one year for the SWIR1 band (Fig.). For NIR reflectance, on the other hand, the disturbance is more often best modelled with a disturbance duration of a single year. This indicates a more immediate influence of bamboo mortality on surface reflectance.

For bamboo populations with two disturbance events, the time between these was typically 27 to 29 years, with a dominance of 28 years (Fig. 9). These pixel-based results confirm scene-based results from previous research which establish a 28-year length of the Guadua bamboo life cycle in southwestern Amazonia (de Carvalho et al., 2013). Because the entire Landsat TM/ETM+ time series covered a time period of 35 years, this life cycle length could only be confirmed for populations with mortality during the first and last few years of the time series. Including Landsat MSS data into this analysis would allow detecting double mortality events for almost all populations in the study site, but this sensor lacks the shortwave infrared band which was found to be the most informative for this purpose. Estimated date of mortality of all populations can now, together with the confirmed life cycle length of 28 years, be used to predict future mortality events and the availability of large fuel volumes.

The outline of the bamboo extent we obtained using the supervised times series analysis visually corresponds quite well with previous delineations of bamboo forests using visual interpretation of Landsat Geocover and MODIS mosaics (de Carvalho et al., 2013) or a linear model using MODIS time series (Dalagnol et al., 2018). With MODIS, one is inherently limited to map bamboo patches with sizes in the order of a square kilometer or larger. Furthermore, the MODIS archive only goes back to 1999, which is shorter than a full flowering cycle of *Guadua* bamboo of approximately 28 years. Manually delineating bamboo populations and their flowering cycle over the entire area using Landsat time series is practically not feasible. In this study, we presented a first attempt to map bamboo-dominated forests and estimate the date of mortality of different bamboo populations automatically at 30 m spatial resolution. We also provided the first validation of a map of bamboo-dominated forests using very high resolution imagery.

We presented here a two-stepped approach to segment Landsat time series and detect the date of bamboo mortality. The first, unsupervised, step is conceptually similar to, e.g., the methodology of De Jong et al. (2013) in that it searches for a segmentation that minimizes the residuals after segmentation, or of Kennedy et al. (2007) in that it is based on the assumption of a distinctive temporal signal before and after the disturbance event, in our case short-term constant and long-term linear signals. As expected, though, the quality of this unsupervised segmentation was poor, with noise in Landsat time series over non-bamboo pixels attributed to change events (Table 1). We therefore attempted a second, supervised time series segmentation using local calibration data. Theoretically, parameters describing disturbance events, e.g. date of disturbance or disturbance magnitude, could be directly obtained from visual interpretation of pixel time series. This set of parameters could then be fed into a supervised segmentation. Unfortunately, such visual time series interpretation, e.g. using the TimeSync software (Cohen et al., 2010), is labour intensive. In the context of bamboo mortality mapping, this is even more so because the spectral response of bamboo mortality differs temporally among bands. This means that a manual extraction of disturbance date and other parameters should be done for each spectral band separately. We therefore suggested a method that extracts calibration samples from the initial, unsupervised time series segmentation using imperfect reference polygons, which are much easier to obtain. A critical condition in our methodology is that at least an important fraction of the pixels within the calibration area are assigned the correct disturbance year in the initial segmentation (Table 1).

We here provided results from analysis run on each of Landsat's infrared bands individually. In recent years, methods have been proposed to improve time series segmentation results by combining outputs from different bands or band indices. These can be roughly divided into two groups: rule-based predictions and stacked generalizations (Healey et al., 2018). The latter relies on accurate reference data to calibrate the ensemble classifier, and is therefore less suitable in the context of bamboo mortality mapping where such reference data is scarce. Future efforts using rule-based approaches could benefit from the findings of our study. E.g., they could use the information in the SWIR1 band to detect where bamboo-dominated forests are present, and the information in the NIR band to detect the actual date of bamboo mortality. The main limitations when using historic Landsat data for the automatic classification of bamboo-dominated forests are data availability and data quality. As a result of historic acquisition and storage policies and frequent cloud cover over Amazonia, several parts of the study area have five or more missing observations in the yearly composite images (Fig 5 (a)). Areas where two or more consecutive yearly composite observations are missing (Fig 5 (b)) are especially problematic since the methodology presented here only allows for a single missing observation over the duration of the disturbance segment (Fig. 4 (a)). Scarcity of Landsat images and excessive atmospheric contamination also contribute to high noise levels in pixel time series, and hence a low DSNR (Fig. 6). This high relative noise level can lead to misleading results when deconstructing the pixel time series into a small number of segments in an unsupervised way. E.g., for the sample pixel time series provided in Fig. 3, dividing the time series into two linear segments from the start of the time series up to 1999 and from 2000 to the end of the time series results by far in the strongest decrease of the residuals. However, from visual assessment we found that bamboo mortality for this and surrounding pixels occurs in 1989. Thus, the best model fit does not necessarily result in the detection of the feature of interest. When incorporating information obtained from calibration data, however, the correct year of disturbance is obtained. Bamboo-dominated forests in southwestern Amazonia are typically considered as consisting of large, homogeneous patches of *Guadua* populations that flower, bear fruits and die back synchronously. Results of this study may suggest that the flowering and mortality rhythms within one bamboo population are more diffuse. When looking at the modelled date of start of disturbance at the scale of the entire study site (Fig. 7), distinct areas can be discerned of several tens of kilometers in diameter with a similar disturbance year. When focussing on one such patch, however, it is often observed that disturbance dates of individual pixels differ one or two years internally. Such internally heterogeneous mortality timing is much harder to identify when using only low resolution data such as MODIS, or when manually digitizing bamboo patches. While part of this within-patch heterogeneity can be attributed to the way the yearly pixel-based composites are created, this hypothesis of asynchronous die-back within patches is corroborated by anecdotal field evidence where we observed bamboo individuals in different life stages (fruiting, flowering, dead and as 1 m high seedlings) at the same site. This hypothesis could be further tested using additional field surveys and repeated very high resolution remote sensing observations.

6. Conclusions

We present a supervised Landsat TM/ETM+ time series analysis to create the first automatic mapping of bamboo-dominated forests in southwestern Amazonia at 30 m resolution, and to identify mortality dates of the different bamboo populations in the area. Analysis using the SWIR1 band resulted in the highest classification accuracy among the three infrared bands, but the spectral response in these wavelengths appeared to lag behind the actual bamboo mortality. The spectral response to bamboo mortality in the shortwave infrared often spanned several years, which reflects the time required for dead bamboo

material to decompose and disappear from the canopy. Using Landsat time series of yearly composite images from 1984 until 2018 we were able to detect several pixels with two bamboo mortality events and derive a typical growing cycle length of 28 years.

Declaration of Competing Interest

The authors report no declarations of interest.

Acknowledgements

Funding for this research was provided through an Academy of Finland grant to RK (grant nr 296406). We made use of computing resources provided by the Open Geospatial Information Infrastructure for Research (oGIIR, urn:nbn:fi:research-infras-2016072513) funded by the Academy of Finland, and by CSC – IT Center for Science, Finland. Fatih Kayaanan provided the visual interpreation of Landsat time series calibration data. We thank two anonymous reviewers for valuable comments.

Appendix A. Supplementary Data

Supplementary data associated with this article can be found, in the online version, at https://doi.org/10.1016/j.jag.2020.102196.

References

Banskota, A., Kayastha, N., Falkowski, M.J., Wulder, M.A., Froese, R.E., White, J.C., 2014. Forest Monitoring Using Landsat Time Series Data: A Review. Canadian Journal of Remote Sensing 40, 362–384.
Bolton, D.K., Coops, N.C., Hermosilla, T., Wulder, M.A., White, J.C., 2018. Evidence of vegetation greening at alpine treeline ecotones: three decades of Landsat spectral trends informed by lidar-derived vertical structure. Environmental Research Letters 13, 084022.
Bullock, E.L., Woodcock, C.E., Olofsson, P., 2020. Monitoring tropical forest degradation using spectral unmixing and Landsat time series analysis. Remote Sensing of Environment 238, 110968.
de Carvalho, A.L., Nelson, B.W., Bianchini, M.C., Plagnol, D., Kuplich, T.M., Daly, D.C., 2013. Bamboo-Dominated Forests of the Southwest Amazon: Detection, Spatial Extent, Life Cycle Length and Flowering Waves. PLOS ONE 8, e54852.
Chow, G.C., 1960. Tests of Equality Between Sets of Coefficients in Two Linear Regressions. Econometrica 28, 591–605.
Cohen, W.B., Healey, S.P., Yang, Z., Stehman, S.V., Brewer, C.K., Brooks, E.B., Gorelick, N., Huang, C., Hughes, M.J., Kennedy, R.E., Loveland, T.R., Moisen, G.G., Schroeder, T.A., Vogelmann, J.E., Woodcock, C.E., Yang, L., Zhu, Z., 2017. How Similar Are Forest Disturbance Maps Derived from Different Landsat Time Series Algorithms? Forests 8, 98.
Cohen, W.B., Yang, Z., Healey, S.P., Kennedy, R.E., Gorelick, N., 2018. A LandTrendr multispectral ensemble for forest disturbance detection. Remote Sensing of Environment 205, 131–140.
Cohen, W.B., Yang, Z., Kennedy, R., 2010. Detecting trends in forest disturbance and recovery using yearly Landsat time series: 2. TimeSync - Tools for calibration and validation. Remote Sensing of Environment 114, 2911–2924.
Curtis, P.G., Slay, C.M., Harris, N.L., Tyukavina, A., Hansen, M.C., 2018. Classifying drivers of global forest loss. Science 361, 1108–1111.
Dalagnol, R., Wagner, F.H., Galvão, L.S., Nelson, B.W., Aragão, L.E.O.e.C.d, 2018. Life cycle of bamboo in the southwestern Amazon and its relation to fire events. Biogeosciences 15, 6087–6104.
De Jong, R., Verbesselt, J., Zeileis, A., Schaepman, M.E., 2013. Shifts in Global Vegetation Activity Trends. Remote Sensing 5, 1117–1133.
DeVries, B., Decuyper, M., Verbesselt, J., Zeileis, A., Herold, M., Joseph, S., 2015. Tracking disturbance-regrowth dynamics in tropical forests using structural change detection and Landsat time series. Remote Sensing of Environment 169, 320–334.
DeVries, B., Pratihast, A.K., Verbesselt, J., Kooistra, L., Herold, M., 2016. Characterizing Forest Change Using Community-Based Monitoring Data and Landsat Time Series. PLoS ONE 11.
Flood, N., 2013. Seasonal composite Landsat TM/ETM+ images using the medoid (a multi-dimensional median). Remote Sensing 5, 6481–6500.
Flood, N., Danaher, T., Gill, T., Gillingham, S., 2013. An operational scheme for deriving standardised surface reflectance from Landsat TM/ETM+ and SPOT HRG imagery for eastern australia. Remote Sensing 5, 83–109.
Galvão, L., dos Santos, e.S.J., Roberts, a.R., Breunig, D.A., Toomey, F.M., de Moura, M.Y.M., 2011. On intra-annual EVI variability in the dry season of tropical forest: A case study with MODIS and hyperspectral data. Remote Sensing of Environment 115, 2350–2359.
Hansen, M.C., Potapov, P.V., Moore, R., Hancher, M., Turubanova, S.A., Tyukavina, A., Thau, D., Stehman, S.V., Goetz, S.J., Loveland, T.R., Kommareddy, A., Egorov, A., Chini, L., Justice, C.O., Townshend, J.R.G., 2013. High-Resolution Global Maps of 21st-Century Forest Cover Change. Science 342, 850–853.
Healey, S.P., Cohen, W.B., Yang, Z., Kenneth Brewer, C., Brooks, E.B., Gorelick, N., Hernandez, A.J., Huang, C., Joseph Hughes, M., Kennedy, R.E., Loveland, T.R., Moisen, G.G., Schroeder, T.A., Stehman, S.V., Vogelmann, J.E., Woodcock, C.E., Yang, L., Zhu, Z., 2018. Mapping forest change using stacked generalization: An ensemble approach. Remote Sensing of Environment 204, 717–728.
Hermosilla, T., Wulder, M.A., White, J.C., Coops, N.C., Hobart, G.W., 2015. Regional detection, characterization, and attribution of annual forest change from 1984 to 2012 using Landsat-derived time-series metrics. Remote Sensing of Environment 170, 121–132.
Karger, D.N.O., Bohner, C., Kawohl, J., Kreft, T., Soria-Auza, H., Zimmermann, R.W., Linder, N.E., Kessler, H.P.L.M., 2017. Climatologies at high resolution for the earth's land surface areas. Scientific Data 1, 170122.
Kennedy, R.E., Cohen, W.B., Schroeder, T.A., 2007. Trajectory-based change detection for automated characterization of forest disturbance dynamics. Remote Sensing of Environment 110, 370–386.
Kennedy, R.E., Yang, Z., Cohen, W.B., 2010. Detecting trends in forest disturbance and recovery using yearly Landsat time series: 1. LandTrendr - Temporal segmentation algorithms. Remote Sensing of Environment 114, 2897–2910.
Kesler, D.C., Walker, R.S., 2015. Geographic distribution of isolated indigenous societies in amazonia and the efficacy of indigenous territories. PLOS ONE 10, e0125113.
Masek, J.G.M., Vermote, E.F., Saleous, N.E., Wolfe, R., Hall, F.G., Huemmrich, K.F., Gao, F., Kutler, J., Lim, T., 2006. A Landsat surface reflectance dataset for North America, 1990-2000. IEEE Geoscience and Remote Sensing Letters 3, 68–72.
Müller, H., Rufin, P., Griffiths, P., de Barros Viana Hissa, L., Hostert, P., 2016. Beyond deforestation: Differences in long-term regrowth dynamics across land use regimes in southern Amazonia. Remote Sensing of Environment 186, 652–662.
Nagol, J.R., Sexton, J.O., Kim, D.H., Anand, A., Morton, D., Vermote, E., Townshend, J.R., 2015. Bidirectional effects in Landsat reflectance estimates: Is there a problem to solve? ISPRS Journal of Photogrammetry and Remote Sensing 103, 129–135.
Nelson, B., Bianchini, M., 2005. Complete life cycle of southwest amazon bamboos (guadua spp) detected with orbital optical sensors. In: in: Anais XII Simpósio Brasileiro de Sensoriamento Remoto. Goiânia, Brasil, 16-21 abril 2005, INPE. pp. 1629–1636.
Pengra, B.W., Stehman, S.V., Horton, J.A., Dockter, D.J., Schroeder, T.A., Yang, Z., Cohen, W.B., Healey, S.P., Loveland, T.R., 2019. Quality control and assessment of interpreter consistency of annual land cover reference data in an operational national monitoring program. Remote Sensing of Environment 111261.
Schroeder, T.A., Schleeweis, K.G., Moisen, G.G., Toney, C., Cohen, W.B., Freeman, E.A., Yang, Z., Huang, C., 2017. Testing a Landsat-based approach for mapping disturbance causality in U.S. forests. Remote Sensing of Environment 195, 230–243.
Song, X.P., Hansen, M.C., Stehman, S.V., Potapov, P.V., Tyukavina, A., Vermote, E.F., Townshend, J.R., 2018. Global land change from 1982 to 2016. Nature 560, 639–643.
Toivonen, T., Kalliola, R., Ruokolainen, K., Malik, R.N., 2006. Across-path DN gradient in Landsat TM imagery of Amazonian forests: A challenge for image interpretation and mosaicing. Remote Sensing of Environment 100, 550–562.
Townshend, J.R., Masek, J.G., Huang, C., Vermote, E.F., Gao, F., Channan, S., Sexton, J.O., Feng, M., Narasimhan, R., Kim, D., Song, K., Song, D., Song, X.P., Noojipady, P., Tan, B., Hansen, M.C., Li, M., Wolfe, R.E., 2012. Global characterization and monitoring of forest cover using Landsat data: opportunities and challenges. International Journal of Digital Earth 5, 373–397.
Van doninck, J., Tuomisto, H., 2017a. Evaluation of directional normalization methods for Landsat TM/ETM+ over primary Amazonian lowland forests. International Journal of Applied Earth Observation and Geoinformation 58, 249–263.
Van doninck, J., Tuomisto, H., 2017b. Influence of Compositing Criterion and Data Availability on Pixel-Based Landsat TM/ETM+ Image Compositing Over Amazonian Forests. IEEE Journal of Selected Topics in Applied Earth Observations and Remote Sensing 10, 857–867.
Van doninck, J., Tuomisto, H., 2018. A landsat composite covering all amazonia for applications in ecology and conservation. Remote Sensing in Ecology and Conservation 4, 197–210.
Woodcock, C.E., Allen, R., Anderson, M., Belward, A., Bindschadler, R., Cohen, W., Gao, F., Goward, S.N., Helder, D., Helmer, E., Nemani, R., Oreopoulos, L., Schott, J., Thenkabail, P.S., Vermote, E.F., Vogelmann, J., Wulder, M.A., Wynne, R., 2008. Free access to Landsat imagery. Science 320, 1011.
Wulder, M.A., White, J.C., Loveland, T.R., Woodcock, C.E., Belward, A.S., Cohen, W.B., Fosnight, E.A., Shaw, J., Masek, J.G., Roy, D.P., 2016. The global Landsat archive: Status, consolidation, and direction. Remote Sensing of Environment 185, 271–283.
Zhu, Z., Wulder, M.A., Roy, D.P., Woodcock, C.E., Hansen, M.C., Radeloff, V.C., Healey, S.P., Schaaf, C., Hostert, P., Strobl, P., Pekel, J.F., Lymburner, L., Pahlevan, N., Scambos, T.A., 2019. Benefits of the free and open Landsat data policy. Remote Sensing of Environment 224, 382–385.